Available online at www.sciencedirect.com
SCIENCE DIRECT
Polymer 46 (2005) 7255–7265
polymer
www.elsevier.com/locate/polymer

Crystallization of ultrathin poly(ε-caprolactone) films in the presence of residual solvent, an in situ atomic force microscopy study

Vincent H. Mareau[a], Robert E. Prud'homme[b,*]

[a]Department of Chemistry, CERSIM, Laval University, Qué., Canada G1K 7P4
[b]Department of Chemistry, University of Montréal, 2900, Boul. Edouard-Montpetit, CP 6128, Downtown Area, Montréal, Que., Canada H3C 3J7

Received 30 March 2005; received in revised form 1 June 2005; accepted 13 June 2005
Available online 19 July 2005

Abstract

The influence of minute amounts of residual tetrahydrofuran on the crystallization of ultrathin poly(ε-caprolactone) (PCL) films has been investigated in real-time by atomic force microscopy. Crystallizations were performed at 30 °C, after melting at 64 °C, for different periods of time; both the morphology and growth rate of the crystals were found to depend on the thermal history of the sample, i.e. on the heating time, due to the evaporation of the residual solvent trapped in the spin-coated polymer. The residual solvent, acting as a plasticizer, facilitates the diffusion of the polymer chains to the crystal growth front; its elimination slows down the growth rates and leads to a decrease of the width of the dendrites. Growth rates were measured for the edge-on and for the flat-on lamellae, which are nucleated from them. Edge-on lamellae were found to crystallize 15 times faster than flat-on lamellae. Finally, spinodal dewetting was observed in the melt left between dendrites grown at 30 °C, after evaporation of the residual solvent, on a substrate of lower wettability. These observations are discussed in terms of the mobility of polymer chains in the melt.

Keywords: Ultrathin films; Crystallization; PCL

1. Introduction

A better understanding of the behavior of ultrathin films of semicrystalline polymers can be of interest for potential nanotechnological applications [1], and in the more fundamental field of polymer crystallization since, in general, they behave differently than thick films. Indeed, several studies have shown that, in ultrathin films, the glass transition temperature [2], the kinetics of crystallization, the degree of crystallinity [1,3–5], and the morphology [5,6], to name only a few properties, can differ significantly from those observed in thick films.

Spin coating is a very common method to produce thin and ultrathin polymer films [7,8]. During this process, after the deposition of the polymer solution on the substrate, the assembly is subjected to a high rotation rate, which eliminates most of the solution due to centrifugal forces; solvent evaporation is responsible for the ulterior thinning of the polymer film. In most of the studies on spin-coated films, the residual solvent trapped in the films after spin coating is removed in a vacuum oven, with or without heating. However, heating ultrathin polymer films above their glass transition or melting temperature can lead to film dewetting. Several studies aimed at the suppression of the dewetting [9] whereas others found in the dewetting phenomenon a method to pattern polymer films at a nanometer scale [10,11].

Two different types of dewetting are observed, differing by their nucleation step. In the first one, called nucleated dewetting, which is the main nucleation process observed in thin films, holes are nucleated by a particle, an impurity in the film, or a defect at the surface of the substrate. After nucleation, the holes grow until their rims merge together, which results in a cellular pattern, and the breakage of the rims results into isolated drops of polymer on the substrate [12–14]. In ultrathin films, spinodal dewetting can also be observed [15,16], with holes showing up simultaneously on all the film surface, turning the film into microscopic droplets. It proceeds by the amplification of the surface

* Corresponding author. Tel.: +1 514 343 6730; fax: +1 514 343 7586.
E-mail addresses: vmareau@chm.ulaval.ca (V.H. Mareau), re.prud-homme@umontreal.ca (R.E. Prud'homme).

0032-3861/$ - see front matter © 2005 Elsevier Ltd. All rights reserved.
doi:10.1016/j.polymer.2005.06.036

disturbance on the free surface of the film, which originates from thermal undulations.

In a previous work, we reported the influence of film thickness on the crystallization of thin and ultrathin poly(ε-caprolactone) (PCL) films [5], for film thicknesses ranging from 200 to 1 nm. In that range, growth rates, melting behaviors and morphologies of the lamellar crystals were found to depend on film thickness. We also observed, at film thicknesses of the order of 1–15 nm, very different morphologies (variation of the width of the dendritic branches, total or partial crystallization of the melt) for films crystallized at room temperature, by changing the thermal history. This was the starting point of the present study in which the influence of the heating time on the morphology and kinetics of ulterior isothermal crystallization of ultrathin PCL films is investigated in real-time by atomic force microscopy. Before the crystallization at 30 °C, films were usually melted at 64 °C for various periods of time, and morphological and kinetic variations were observed. The results are discussed in terms of the variation of the amount of residual solvent present in the films, which influences the diffusion of the polymer chains from the melt to the growing crystal, and the wetting properties of the films.

For this study, for practical reasons, we have chosen a film thickness of 6 nm since, the crystallization of thinner films is too slow whereas thicker films crystallize too fast to allow a good observation. These results are certainly valid both for thinner and thicker films. In addition, at this specific thickness, the large difference of growth rates between flat-on and edge-on lamellae nucleated by the AFM tip can be illustrated.

2. Experimental section

2.1. Materials

Poly(ε-caprolactone) (PCL, $M_n = 39{,}000$ and $M_w/M_n = 1.4$) was purchased from Aldrich Chemicals, and used without further purification. Its molecular weight was determined by gel permeation chromatography absolute molar mass determination. The glass transition temperature (T_g) and melting point of PCL were found to be −60 and 60 °C, respectively, using a Perkin–Elmer DSC-7 calorimeter at a heating rate of 20 °C/min. In order to prepare ultrathin films, PCL was dissolved in tetrahydrofuran (THF) for at least 4 h, at room temperature and in the absence of light.

2.2. Sample preparation

Six nanometers ultrathin PCL films were prepared by spin coating a solution of PCL in THF at a concentration of 1.0 mg/ml onto cleaned Si substrates (p-type single-side polished (100) silicon wafers) using a Headway Research Inc, EC101 spin coater at 3000 rpm during 60 s. Si substrates were cleaned by immersion in a sulfochromic acid solution for 2 min to remove any organic contamination and, also, to hydroxylate the native oxide layer thus, making the surface hydrophilic [17] (sulfochromic acid should be handled and neutralized with care). Static contact angles measured with glycerol decreased from 33° for as-received substrates down to $<5°$ after sulfochromic treatment. The substrates were then rinsed with nanopure water and dried by spinning for 80 s at 3000 rpm and, finally, by heating in a 500 W domestic microwave oven for 90 s. The substrate was allowed to cool before spin coating the PCL solution. To keep a solvent saturated atmosphere around the sample and to allow a uniform evaporation, a glass dome was placed on top of the sample area during spin coating. As high relative humidity leads to dewetting during spin coating, the spin coater was placed in a customized epoxy box flushed with dry air before spin coating, to reduce the relative humidity below 8%. Film thicknesses were measured by profilometry using AFM [18]. All samples characterized in this paper have a thickness of 6 ± 1 nm.

2.3. Atomic force microscopy

A nanoscope III multimode AFM (Digital Instruments (DI), Santa Barbara, CA), operated in tapping mode and equipped with a high-temperature heater accessory (DI) was used to capture images at 30 °C, after heating at 64 or 90 °C for different periods of time. A J-scanner was used with RTESP silicon probes (nanoprobes). Temperature calibration of the hot-stage was verified both with a thermocouple and a pure benzophenone sample of known melting point (48 °C). As the film thickness investigated here is below the 500 nm limit found by Schönherr et al. [19] for PEO, it was assumed that the temperature of the sample was not influenced by the film thickness and was equal to the temperature read on the hot-stage controller.

3. Results and discussion

3.1. Crystallization at 30 °C after melting for a short time

In Fig. 1(a)–(d), four AFM height images were taken on the same area of the film ($25 \times 25\ \mu m^2$), at four different times, to illustrate the crystallization process at 30 °C (after melting for 1 min at 64 °C). The crystallization leading to Fig. 1(a)–(d) was done after melting the sample for 1 min at 64 °C. This limited melting time is long enough to melt the crystals grown in the 2 min interval between the spin-coating of the sample and the AFM observation, but short enough to retain a significant amount of residual THF. PCL crystals show a dendritic morphology, with lamellae growing with a flat-on orientation after an initial edge-on growth, a phenomenon already observed for poly(lactide) [20,21] and for isotactic poly(styrene) [22]. Single edge-on

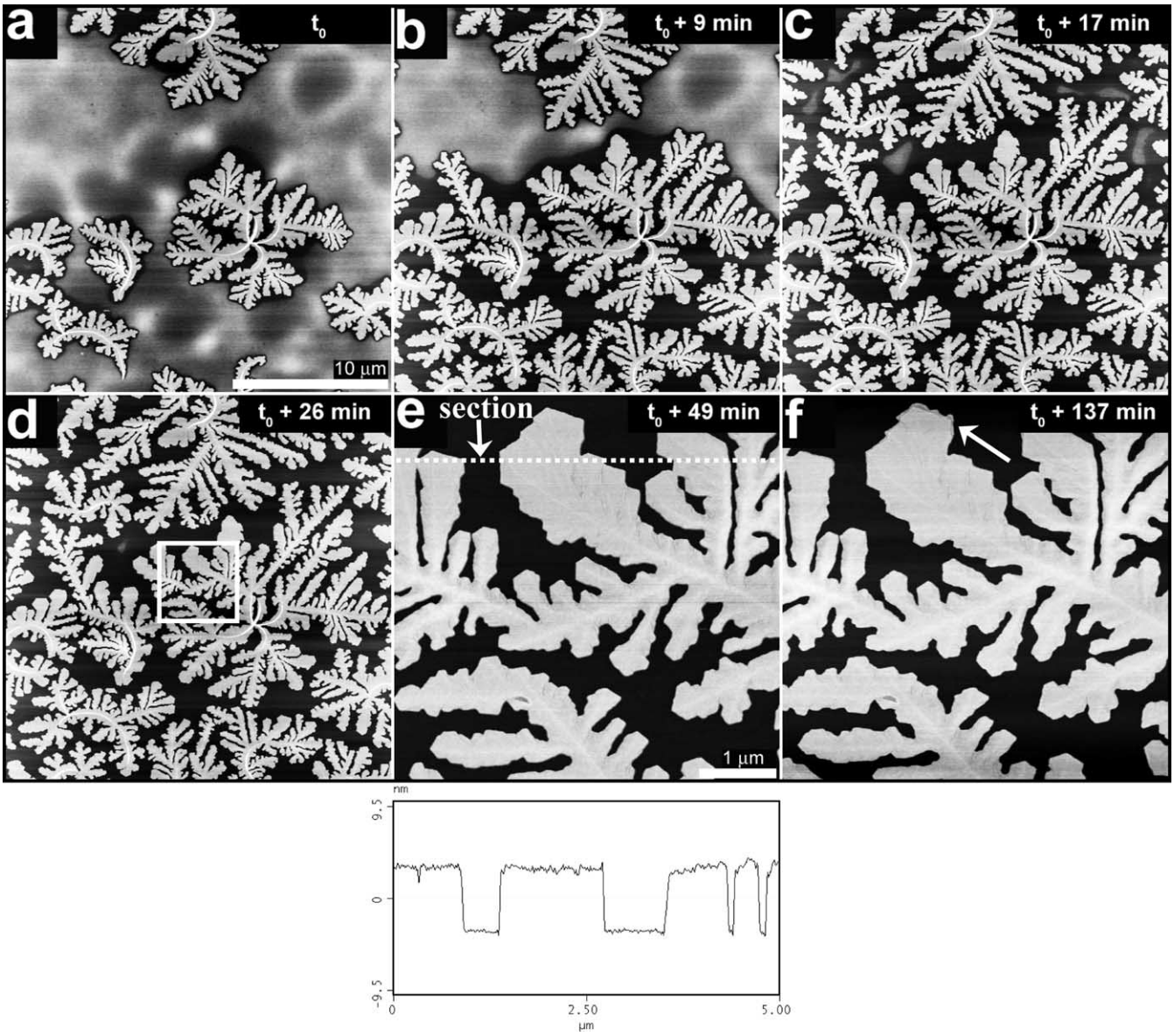

Fig. 1. Tapping mode height AFM images of a 6 nm PCL film, isothermally crystallized at 30 °C after 1 min at 64 °C: (a)–(d) are 25×25 µm^2 images and (e) and (f) are 5×5 µm^2 images corresponding to the area indicated by a white square in (d). A cross section corresponding to the white dotted line is given below (e), (f) was taken after a short period of time below 0 °C.

lamellae are recognized as white thin strips at the center of the crystals; they appear white due to their higher topography (about 15 nm) as compared to the flat-on lamellae surrounding them which are 7–8 nm thick. The width of the edge-on lamellae should logically correspond to the thickness of the flat-on lamellae, i.e. 7–8 nm. However, as the edge-on lamellae are surrounded by flat-on lamellae, which evolve from them, no accurate measurement could be made by AFM. Growth rates of the edge-on lamellae could not be measured from this set of AFM images, as they appeared before we took the first AFM image, but additional information about edge-on growth are given later in the text.

The flat-on orientation of the dendrites observed in PCL films is demonstrated by their homogeneous thickness, and was already established by electron diffraction in a previous paper [5]. Indeed, the electron diffraction patterns obtained from such dendritic crystals exhibit diffraction spots corresponding to the (hk0) projection of the reciprocal lattice of the PCL structure. The preferred growth directions of primary branches, or angular relationship between primary and secondary branches were not determined as the very small film thickness and low melting temperature of PCL (poor resistance under the electron beam) inhibit such detailed analysis.

Linear growth rates could be measured for a short period of time, at the beginning of the crystallization, for dendrite branches sufficiently isolated to grow free from interference

with other branches, as the competition between growing branches reduces the growth rates (this precaution will be applied to all growth rate measurements of this study). An uncertainty of about 20% must be considered due to the large variation of G from branches to branches in a given sequence of images. The average growth rate in Fig. 1 is about 11 nm/s, decreasing rapidly as the melt is consumed by the crystals, which is observed in Fig. 1(a)–(d) with depleted 'black' areas surrounding the growth fronts, with only a small amount of melt remaining available in Fig. 1(d), taken 26 min after Fig. 1(a). Therefore, we must conclude that the melt can diffuse over long distances (several micrometers) to crystallize at the growth front of the crystals since, after a period of time of less than 1 h, no more melt is observed by AFM between the dendrite branches, the crystallization being then completed. This phenomenon is shown in Fig. 1(e) and (f), corresponding to an enlargement of the area indicated in Fig. 1(d) by a white square. Fig. 1(e) was taken 49 min after Fig. 1(a), and no melt can be observed between the dendrites, as shown by the cross-section presented below Fig. 1(e) and corresponding to the white dotted line drawn on Fig. 1(e).

In order to verify if PCL melt was left between the dendrite branches of Fig. 1(e), an attempt was made to crystallize this sample in the AFM slightly below 0 °C. For all practical purposes, no more crystallization was seen (except at the spot indicated by an arrow at the top of Fig. 1(f)), confirming the interpretation of the previous images.

3.2. Crystallization at 30 °C after melting for a long time

A similar experiment was made with a longer heating time of 41 h at 64 °C, before the crystallization at 30 °C. In Fig. 2(a)–(c), three AFM height images were taken, on the same area of the film ($25 \times 25\ \mu m^2$), at three different times. The dendritic lamellae, growing in a flat-on orientation, have a thickness between 7 and 8 nm, as in Fig. 1, but their morphology is very different from those of Fig. 1, with branches obviously narrower. In addition, no edge-on lamellae are observed in Fig. 2 at the center of the dendritic crystals, contrary to Fig. 1. A longer heating time decreases the probability of generation of spontaneous edge-on lamellae (nucleated in areas untouched by the AFM tip) but it was possible to observe edge-on lamellae in the same sample, nucleated by the forces applied by the AFM tip on the melted polymer. Other differences between the two figures are lower growth rates of about 5 nm/s, almost half of the 11 nm/s observed in Fig. 1, and the absence of large depleting black areas surrounding the growing crystals, indicating that there is no consumption of melted polymer over large distances. Instead, the thickness of the melted polymer observed between the growing dendrites is homogeneous, even at the proximity of the dendrites.

Fig. 2(d) is a magnification of the area indicated by a white square ($5 \times 5\ \mu m^2$) in Fig. 2(c). This zoom view of the dendrites indicates that the depletion area of the melted film in the vicinity of the dendrites is large of a few tens of nanometers only, as illustrated by the cross-section shown below Fig. 2(d) and corresponding to the white dotted line drawn on the AFM image. Fig. 2(e) was taken nearly 2 days later, almost at the same position as Fig. 2(d). It is seen that the growth of the dendrites has been very limited. Fig. 2(f) was taken at the same position, but after a short period of time at a lower temperature, i.e. below 5 °C, which enables nucleation to take place in the melted layer, and leads to the crystallization of very small dendrites, observed in Fig. 2(f). This is the proof (1) that there is melted polymer remaining between the dendrites, and (2) that it can crystallize, even if the crystallization does not occur over long distances and does not consume all the melted polymer available.

The differences observed in growth rate and crystal morphology between Figs. 1 and 2 cannot be due to the thermal degradation of the PCL because the melting temperature used in this study, 64 °C, is just above the PCL melting temperature, and far from the temperatures at which thermogravimetric analysis can detect a thermal degradation of the PCL, about 200 °C [23]. Therefore, it is assumed that the evaporation of residual THF present in the ultrathin films after spin coating is responsible for this phenomenon. We tried to detect the presence of residual THF in the ultrathin films by Raman confocal microscopy and infra-red spectroscopy, but without success due to the thickness of the film and the very small quantity of residual solvent to be measured.

The residual THF in PCL ultrathin films can act as a plasticizer, making the diffusion of the polymer chains faster and easier. This explains why the growth rate decreases with an increase of heating time and, therefore, a decrease of the residual THF. In addition, as shown in Fig. 1, when THF is present, all the polymer chains found between the dendrites can diffuse to the growth front and crystallize whereas, after a long heating time of the sample at 64 °C, the amorphous polymer found between the dendrites has great difficulty to crystallize as shown in Fig. 2.

As shown in Fig. 2, a large decrease of the temperature is needed to nucleate the melted polymer found between the dendrites. In addition, those polymer chains become isolated from the crystal growth front, as their restricted mobility forbids their diffusion through the depletion area, which finally becomes a gap impossible to cross. A step of homogeneous nucleation is necessary for the residual melt to crystallize, which is finally achieved with a decrease of the temperature [24,25]. It must be emphasized that larger depletion areas surrounding the crystals growth fronts are observed in Fig. 1 than in Fig. 2, as the larger mobility of the polymer chains in Fig. 1 allows their diffusion from larger distances. However, these large depletion areas do not stop the crystallization process, as PCL chains can diffuse through larger depletion areas in presence of residual THF.

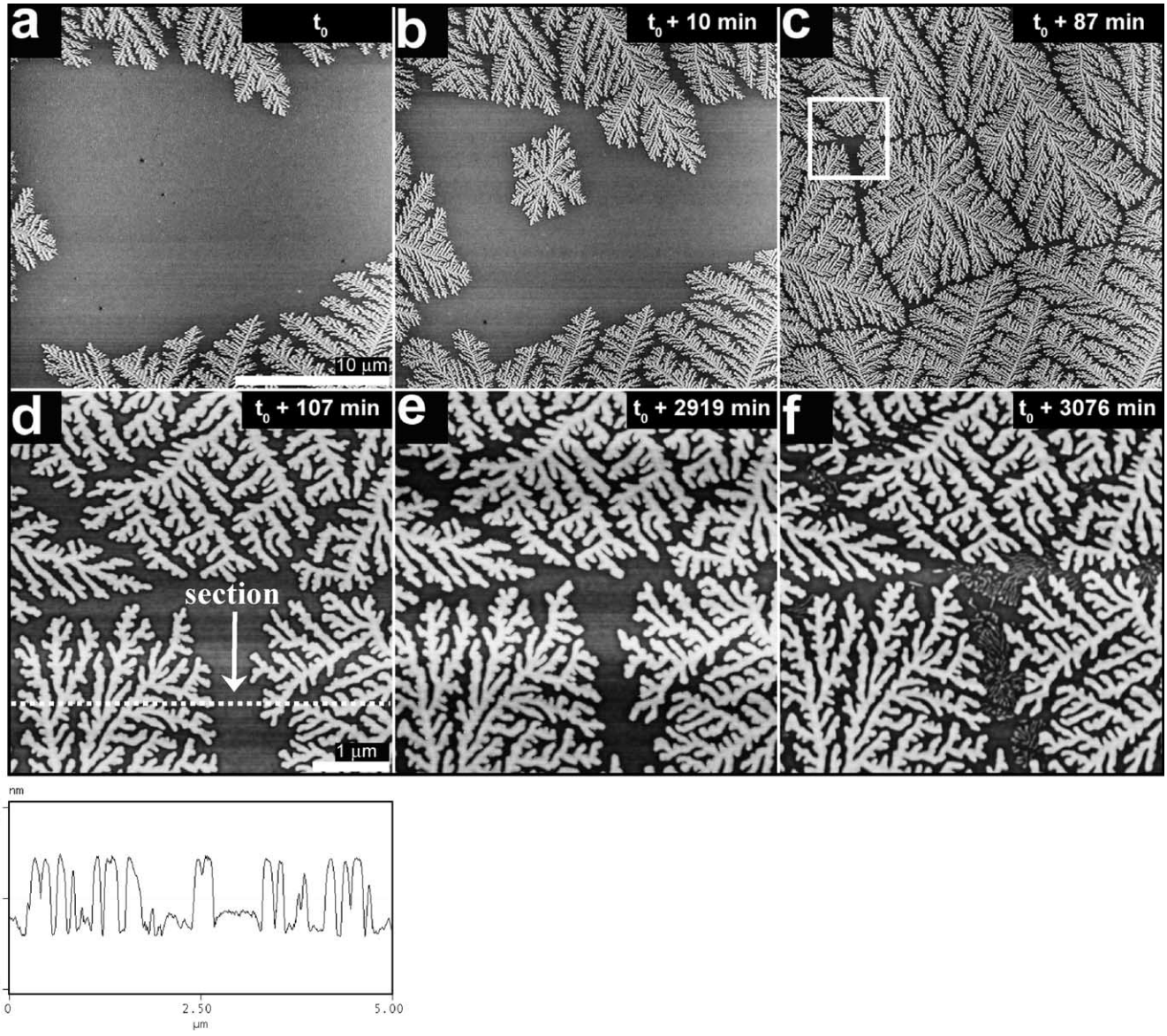

Fig. 2. Tapping mode height AFM images of a 6 nm PCL film, isothermally crystallized at 30 °C after 41 h at 64 °C: (a)–(c) are 25×25 µm^2 images and (d)–(f) are 5×5 µm^2 images corresponding to the area indicated by a white square in (c). A cross section corresponding to the white dotted line is given below (d), (f) was taken after a short period below 5 °C.

3.3. Kinetics and morphology versus thermal history

Fig. 3 shows AFM height images obtained after crystallization following six different thermal histories; the six pictures are at the same scale (surfaces of 10×10 µm^2) making straightforward the comparison of the morphological changes which occur. Fig. 3(a) can be considered as a reference image showing the morphology observed without any heating at 64 °C. Fig. 3(b) clearly demonstrates, in comparison with Fig. 3(a), that the heating at 64 °C for 1 min does not affect significantly the dendritic morphology. However, the dendrite branches of Fig. 3(a) are narrower than those of Fig. 3(b) because the isothermal crystallization was performed at a lower temperature, 22 °C, in Fig. 3(a) as compared to 30 °C in Fig. 3(b).

A direct comparison of the width of the dendritic branches is possible between Fig. 3(b)–(f), as the five morphologies were all recorded at the same crystallization temperature (30 °C), the only variable parameter being the heating time at 64 °C. The regular decrease of the branch width with increasing heating time is obvious.

Growth rates were measured on sequences of AFM images from which Fig. 3(b)–(f) were extracted, and from an additional crystallization at 30 °C, after a heating time of 30 min. Growth rates of 11, 6, 5, 4, 6 and 5 nm/s were measured for heating times of 1, 30 min, 2, 6, 19 and 41 h, respectively, with an uncertainty of about 20%. A decrease by a factor of two is then observed between PCL films heated for only 1 min at 64 °C and the others. However, no clear variation of growth rate was found between films

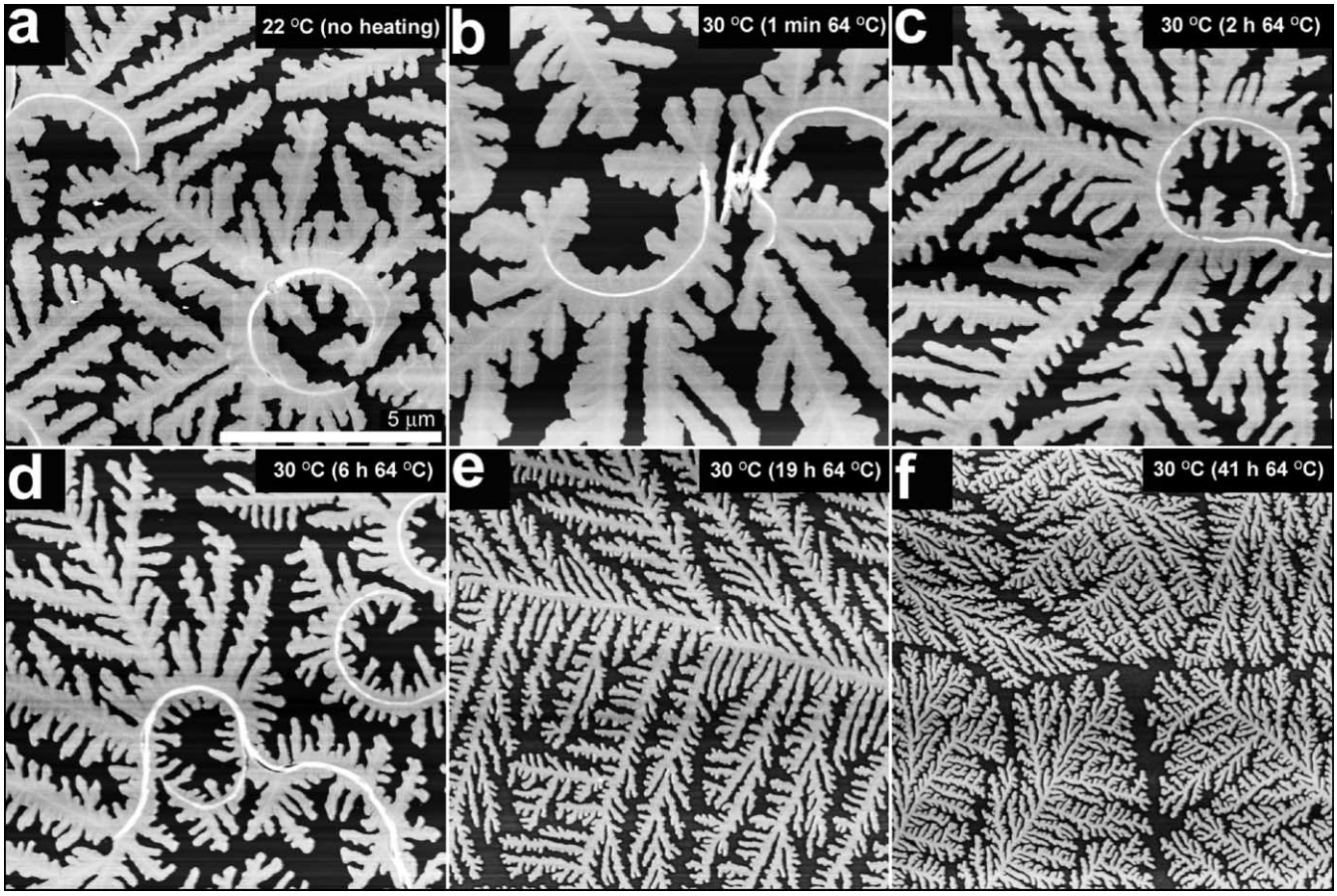

Fig. 3. Tapping mode height AFM images (10×10 μm^2) of 6 nm PCL films isothermally crystallized: (a) at room temperature (22 °C) without any heating at 64 °C; crystallized at 30 °C for the five other images, after heating at 64 °C for: (b) 1 min; (c) 2 h; (d) 6 h; (e) 19 h; (f) 41 h.

heated from 30 min to 41 h, whereas a continuous decrease of the branch width is observed when the heating time is increased. As already mentioned, the evaporation of the residual THF can be responsible for the decrease of the growth rate due to the slower diffusion of the PCL chains; it could also explain the decrease of the dendritic branch width observed. At a given crystallization temperature, the probability of creating secondary nuclei at the growth front is identical, whereas the diffusion of the polymer chains decreases as the heating time increases due to the evaporation of the residual solvent. The combination of these two phenomena leads to a larger number of nuclei spreading slowly at the growth front, as in Regime II of Hoffman et al. [26], (as compared to Regime I), which, at the same time, gives dendrites of smaller width.

If the phenomenological theory of Keith and Padden [27] is applied to the dendritic morphology observed in this study, the parameter $\delta = D/G$ that usually defines the diameter of the fibers observed in spherulites, can be associated to the width of dendritic branches. When the residual THF evaporates from the melt, the diffusion coefficient of the impurities in the melt (D) decreases because THF acts as a plasticizer, and the radial growth rate of the dendrites (G) decreases according to our measurements. For heating times longer than 30 min, where D decreases and G is almost constant, δ tends to decrease. Additional observations would, however, be necessary to verify how the morphology evolves for films heated at 64 °C between 1 and 30 min, to verify if D decreases faster than G, which would also lead to a decrease of δ and, therefore, of the width of dendritic branches, or if the opposite is observed. From our measurements, values of D were estimated to decrease from 33×10^{-12} to 3.5×10^{-12} cm^2/s when increasing the heating time at 64 °C from 1 min to 41 h.

3.4. Edge-on lamellae nucleated by the AFM tip

Edge-on lamellae are seen in Figs. 1 and 3 at the center of the large flat-on dendritic crystals which were nucleated before any contact with the AFM tip. However, their size and density are lower than in AFM scanned areas, and the probability to see spontaneous edge-on orientation decreases as the heating time increases (and as THF evaporates). This behavior may be due to the hydrophilic character of THF, the solvent enabling a more stable contact between the hydrophobic PCL and the hydrophilic substrate.

It was also found that new AFM tips have a poorer capacity to nucleate edge-on lamellae in comparison with used tips, which are certainly covered with polymer and, therefore, interact more strongly with the melt. Edge-on lamellae nucleated by the AFM tip are mostly found at the central horizontal line of the scanned area where the AFM tip engages on the surface, a position where higher forces are applied on the sample. In addition, other edge-on lamellae are nucleated on the defects of the film (impurity or substrate defects) as they are obstacles for the AFM tip and, therefore, the origin of stronger interactions with the melt.

Edge-on lamellae systematically grow first in the direction perpendicular to the fast motion of the tip, i.e. vertically in the AFM images shown in this paper, and in both up and down directions. The nucleation of edge-on lamellae by the shear forces applied by an AFM tip was already described by Vancso et al. [28], Schönherr and Frank [1] and Kikkawa et al. [21], and also proposed as a method to control the lamellar orientation of ferroelectric copolymers [29]. It originates from the fact that polymer chains are dragged by the AFM tip in the fast-scanning direction, and parallel to the substrate. With chains having a similar orientation, the nucleation is favored, with a edge-on orientation, and the edge-on lamellae first grow perpendicular to the fast scanning direction of the AFM tip.

This phenomenon is shown in Fig. 4 by three AFM height images taken on a PCL film heated for 30 min at 64 °C, before crystallization at 30 °C. The three images were taken in the same area of the film (25×25 μm^2), at three different times. From this set of images, it can be seen that the growth rate of the edge-on lamellae is much faster than that of flat-on lamellae. Edge-on lamellae shown in Fig. 4, like those of Figs. 1 and 3, appear to be single lamellae and not bundles of lamellae. Measurements made on these images give an approximate growth rate of 90 nm/s for edge-on lamellae, which is 15 times faster than the 6 nm/s measured for the surrounding flat-on lamellae. As already mentioned, no accurate AFM measurement of the width of the edge-on lamellae was possible due to the presence of the surrounding flat-on lamellae.

The curving motion of the edge-on lamellae sometimes brings the growth front of the lamellae in the direction of an already crystallized area, as observed in Fig. 4. When this happens, the growth of the lamella is suddenly stopped. In Fig. 4, the very long edge-on lamella is also observed to give birth to strongly curved 'daughter' edge-on lamellae.

Similarly, in Fig. 5(a) is shown an AFM image (25×25 μm^2) of a PCL film crystallized at 30 °C after 6 h of heating at 64 °C. In this AFM image, a long edge-on lamella is observed with many daughter edge-on lamellae nucleated along its sides. From the dimensions of the flat-on dendritic lamellae nucleated from the edge-on lamella, it is obvious, here again, that edge-on lamellae grow much faster than the flat-on lamellae originating from them. This difference is due to the ultrathin dimensions of the 6 nm PCL films, even smaller than the lamellar thickness found to be about 7–8 nm. In contrast, Kikkawa et al. [21] did not find any difference between the growth rates of edge-on and flat-on polylactide (PLLA) crystals in 100 nm thick films. However, these two results are not necessarily in contradiction. In the flat-on orientation, the 7–8 nm thick lamellae crystallize with a large growth front (several micrometers) and, therefore, necessitate the diffusion of a large amount of PCL chains to grow. Due to the ultrathin dimensions of the 6 nm films, a depletion area in then created at the growth front, which slows down the growth rate, which does not occur in 100 nm thick films. In the edge-on orientation, the PCL lamellae have a very narrow growth front, with a measured thickness of about 15 nm and a width estimated to be about 7–8 nm (corresponding to the lamellar thickness measured for flat-on lamellae). The number of PCL chains necessary to 'feed' the growth of a edge-on lamella is then small as compared to what is needed for a flat-on lamella. We, therefore, suggest that the depletion area at the growth front of edge-on lamellae is absent or very limited as compared to that surrounding

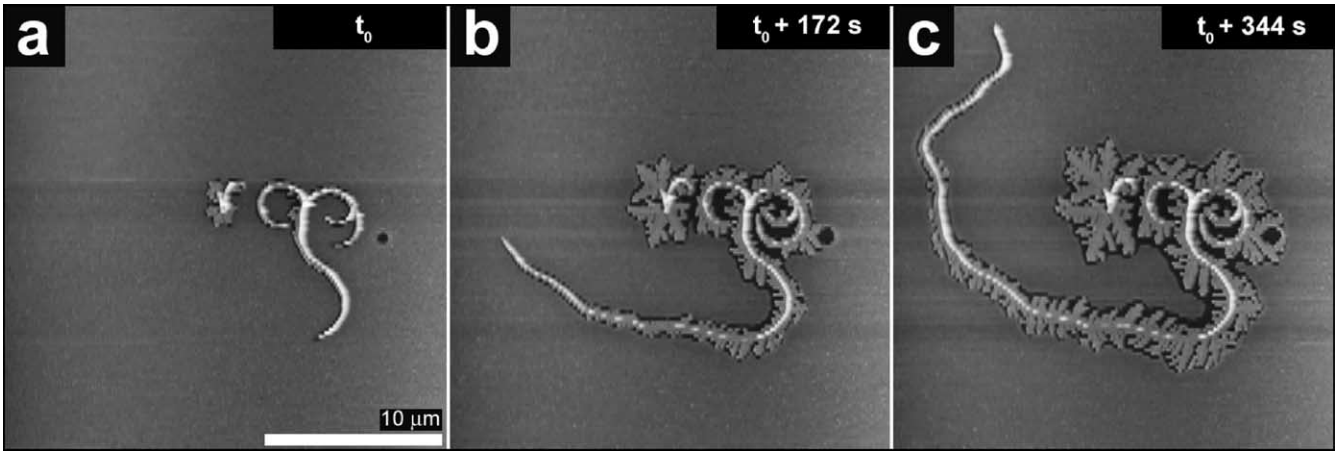

Fig. 4. Tapping mode height AFM images (25×25 μm^2) of a 6 nm PCL film isothermally crystallized at 30 °C after 30 min at 64 °C for (a) 129, (b) 301 and (c) 473 s.

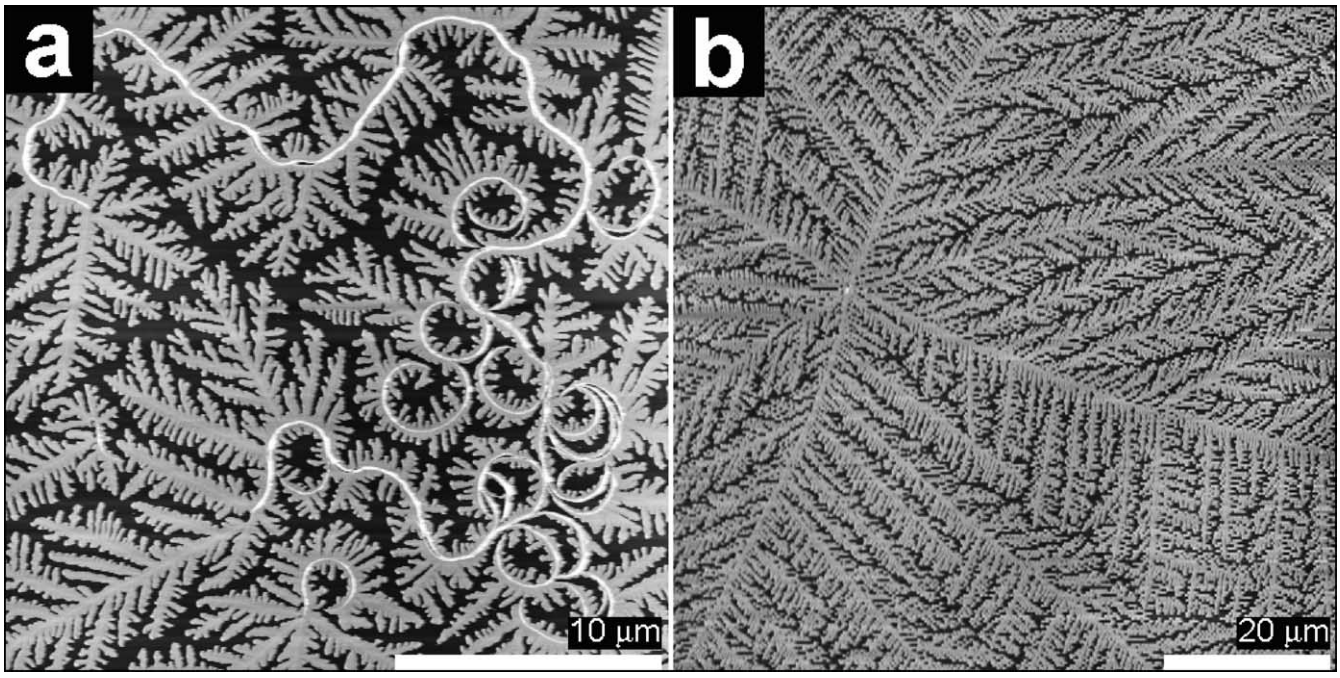

Fig. 5. Tapping mode height AFM images ((a) 25×25 μm^2, and (b) 80×80 μm^2) of a 6 nm PCL film isothermally crystallized at 30 °C after 6 h at 64 °C for (a) 20 h and (b) a few minutes after (a).

flat-on lamellae, a phenomenon already described by Izumi et al. [22] for isotactic poly(styrene). Both the easier access of the polymer chains to the growth front of edge-on lamellae, and their limited needs as compared to flat-on lamellae can explain their faster crystallization.

Nevertheless, the growth rate of edge-on lamellae in 6 nm PCL films does not correspond to the growth rate observed in thick films. For example, PCL spherulites in the bulk grow faster than ultrathin films, at 250 nm/s in 2 μm thick films crystallized at 36 °C [30] (growth rates at 30 °C were too fast to be measured). Therefore, even if edge-on lamellae crystallize faster than flat-on lamellae, their growth rate is still reduced by the slower diffusion of the polymer chains due to the film thickness, as suggested in a previous study [5].

Kikkawa et al. [21] observed the growth of S and C-shaped edge-on lamellae in PLLA thin films, and found that the curvature of edge-on lamellae occurs in arbitrary directions. Our observations of much longer PCL edge-on lamellae confirm this finding, with several changes in direction during the growth. At first, the growth of edge-on lamellae seems to be a random walk but a more careful examination indicates that, once the growth has started to curve in one direction, the probability to keep this direction is very high. Similar curved edge-on lamellae were observed by Keith et al. [31] in polyethylene who associated this phenomenon to the existence of half lamellae, i.e. lamellae 'split' along their growth axis (*b* axis). Indeed, the model previously developed by Keith and Padden [32] to explain the origin of lamellar twisting (related to banded spherulites [33]), assumes that twisted lamellae result from unbalanced surface stresses generated by the chain tilt in the lamellae. This model proposes that unbalanced surface stresses exerted on half-lamellae would induce a lamellar curvature. Based on this model, we can assume that the edge-on lamellae observed in PCL ultrathin films are half-lamellae, which chain tilt changes during the growth, changing the orientation of the curvature. We can also assume that, during their growth, the edge-on lamellae are sometimes symmetrically composed of their two half (when they are straight), and sometimes predominantly composed of their upper or lower half and, therefore, curved in one direction or the opposite. The systematic transition observed from edge-on to flat-on lamellae, and never in the other direction, let us believe that flat-on lamellae are more stable and favored, perhaps due to a lower contact between the polymer chains (hydrophobic) and the substrate (hydrophilic).

Finally, in Fig. 5(b) is given an AFM image (80×80 μm^2) taken on the same sample from which Fig. 5(a) was scanned. This picture shows the fact that flat-on dendritic lamellae can nucleate alone, not necessarily from an edge-on lamella, a phenomenon principally observed when the nucleation occurs outside the AFM scanned-area.

3.5. Dewetting of the melted film and homogeneous nucleation

Two types of dewetting were observed during this study: nucleated dewetting and spinodal dewetting. Humidity can impede the preparation of continuous PCL films as it enhances nucleated dewetting, with large holes appearing

during the heating at 64 °C when the film is more fluid. Frequent nucleated dewetting is also observed when the hydrophilization of the Si surface is not sufficient.

Spinodal dewetting was observed in the melted polymer, between dendrites. This phenomenon is shown in Fig. 6 with a sequence of five AFM height images and one AFM phase image taken on a PCL film, melted for 1 min at 90 °C, then crystallized at 50 °C for 46 h, and finally cooled to 30 °C to achieve further crystallization at this lower temperature (4, 9.7, 23.5, 27, and 1132 h for Fig. 6(a)–(e), respectively). Five different phases can be seen on those images: first, the PCL flat-on single crystals grown at 50 °C with an average thickness of 12 nm, as indicated by the arrow in Fig. 6(a) (taken when the crystallization of the dendrites at 30 °C was stopped and the available melt found between the dendrites had started to dewet); second, the dendritic flat-on crystals grown at 30 °C, with an average thickness of 7 nm; third, the edge-on lamella also crystallized at 30 °C with a horn shape; fourth, the melted polymer found between the crystals; and, finally, the Si substrate observed through the dewetting of the polymer melt.

It should be noted that the dendrites observed in Fig. 6 have a similar morphology as those described in Fig. 2. However, the melted phase found between the dendrites occupies a larger surface in Fig. 6 (the dendrites stopped growing after a shorter growth), which could certainly explain the dewetting observed in Fig. 6 and not in Fig. 2. The shorter dendritic growth can be the result of different thermal histories between Figs. 2 and 6, or from a slightly poorer hydrophilization of the substrate, which can lead to a rupture (dewetting) of the amorphous film at the growth front of the dendrites and, therefore, stop their growth. Actually, the PCL film described in Fig. 6 was favorable to nucleated dewetting, which can also originate from adsorbed water, as this experiment was done without a rigorous humidity control.

The spinodal dewetting process occurs slowly at 30 °C, as shown in Fig. 6(a)–(c). During dewetting the surface occupied by the continuous melted film decreases, whereas its thickness increases. Melted droplets of various sizes are left behind by the melted film as it dewets. Fig. 6(d) was taken at the same position as the previous ones, but after a short period below 10 °C, using the same method as described above. This lower temperature enables nucleation to take place in the melted polymer found between the dendrites, and leads to the crystallization of dendrites

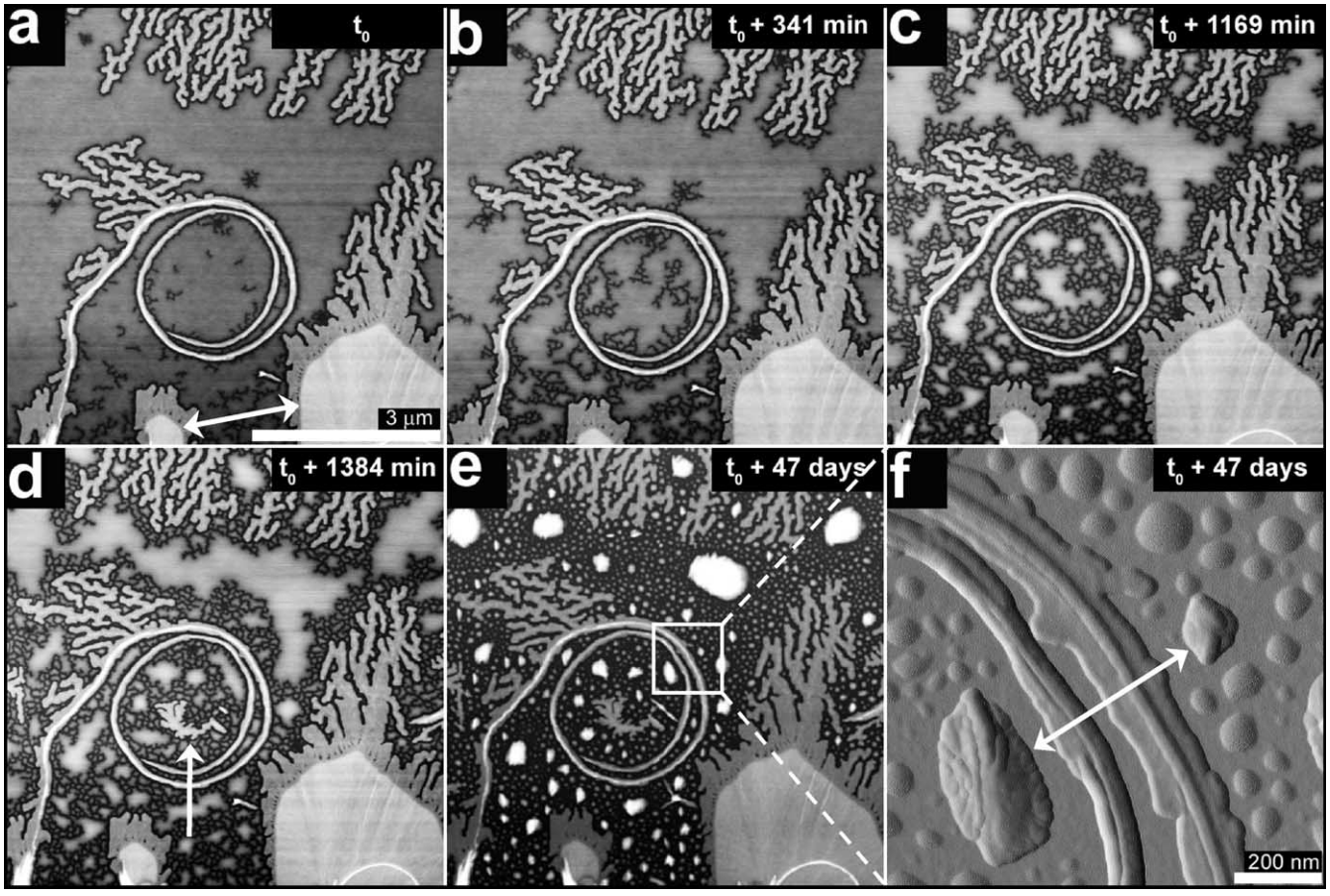

Fig. 6. Tapping mode AFM images of a 6 nm PCL film isothermally crystallized at 30 °C after previous isothermal crystallization at 50 °C, preceded by a heating at 90 °C for 1 min; (a)–(e) are height images (7×7 µm^2) and (f) is a amplitude image (1×1 µm^2), corresponding to the area indicated by a square in (e); (d) was taken after a short period of time below 10 °C, and (e) and (f) after 47 additional days at room temperature.

slightly smaller than those obtained at 30 °C, as indicated in Fig. 6(d) by an arrow.

Fig. 6(e) was taken at the same position as Fig. 6(d), but 47 days later, with the sample kept at room temperature during this long period of time. We can see that the dewetting leads to the formation of melt droplets, and that the larger ones have crystallized, as indicated by their granular morphology compared to the smooth topography of the melt. This phenomenon is more easily observed in Fig. 6(f), an amplitude AFM image which corresponds to the area indicated by a square in Fig. 6(e). In Fig. 6(f), two crystallized droplets are indicated by an arrow, and several smaller droplets still amorphous can be observed on both sides of the edge-on lamella.

The presence of uncrystallized droplets in a PCL sample kept at room temperature for 47 days can be surprising but is easily explained by the very small volume of the droplets and, therefore, the low probability for a homogeneous nucleus to appear in such a small volume. Heterogeneous nucleation can be ruled out at this stage of the crystallization, as it would have appeared earlier, and as impurities are usually found outside the amorphous droplets [24,25]. The homogeneous character of the nucleation observed in the residual melted film, between the dendrites, is confirmed by the large supercooling needed to observe new nuclei, as shown in Figs. 2(f) and 6(d), or by the very long period of time required, as shown in Fig. 6(f).

The results shown in Fig. 6 confirm the influence of the residual THF on the crystallization of ultrathin PCL films. They also indicate that the melted polymer, isolated from crystalline dendrites due to the difficult diffusion of PCL chains, can finally dewet if large surfaces are left amorphous, and if the substrate is slightly less energetic. This behavior is completely different from the complete crystallization observed in Fig. 1, when residual THF was present in the ultrathin film.

4. Conclusions

In summary, the morphology and crystallization kinetics of PCL ultrathin films crystallized at 30 °C have been found to critically depend on thermal history, i.e. on the length of time the films were previously held at 64 °C, slightly above the melting temperature of PCL. Heating times of 30 min or more result in slower crystallizations at 30 °C, as compared to a heating time of 1 min, with growth rates roughly divided by two. Simultaneously, a progressive decrease of the width of dendritic branches is observed, since, an increase of the heating time decreases the amount of residual solvent trapped in the spin-coated films. The residual THF is assumed to act as a plasticizer, and a decrease of its concentration results in a lower mobility for PCL chains.

We also found that spontaneous nucleation of edge-on lamellae decreases with the heating time. However, edge-on lamellae are easily nucleated by the shear forces resulting from the scanning of the AFM tip. Very long edge-on lamellae have been observed to grow 15 times faster than the flat-on lamellae which are nucleated from them.

Finally, a spinodal dewetting has been observed in the melted polymer remaining between dendritic branches crystallized at 30 °C, following a crystallization at 50 °C. The dewetting results from the large surface of the amorphous areas, and the reduced wettability of the substrate due to a poor hydrophilization or the presence of adsorbed water. Isolated amorphous droplets resulting from this dewetting are very difficult to crystallize due to the absence of heterogeneous nuclei.

The ability of the PCL chains to diffuse from the melt to the crystal growth front, and the kinetics of their motions, both depending on the content of residual solvent, have been found to be the key to most of the phenomena described in this study. These phenomena have been observed here in 6 nm thick films for experimental reasons (because thicker and thinner films crystallize too fast and too slowly to allow an easy observation) but it is clear that they apply to most ultrathin films, i.e. those having thicknesses below 15 nm. In thicker films, the difference, for example between the growth rate of edge-on and flat-on lamellae is not seen anymore [21].

The results shown in this paper demonstrate that the morphology found upon the crystallization of ultrathin films can depend on traces of solvent remaining in the film, therefore, it is of outmost importance before the crystallization to select a thermal history that leads to the elimination of all traces of solvent because, otherwise, the morphologies can be difficult to repeat. On the other hand, if needed, the morphologies of ultrathin films can be significantly modified by a very simple method, i.e. the use of the remaining traces of solvent.

Acknowledgements

We thank Dr Bernard Lotz from Institut Charles Sadron, Strasbourg, France, for his useful comments concerning the interpretation of the curvature of edge-on lamellae. This study was supported by NSERC and FCAR grants.

References

[1] Schönherr H, Frank CW. Macromolecules 2003;36:1188.
[2] Forrest JA, Dalnoki-Veress K. Adv Colloid Interface Sci 2001;94:167.
[3] Frank CW, Rao V, Despotopoulou MM, Pease RFW, Hinsberg WD, Miller RD, et al. Science 1996;273:912.
[4] Sawamura S, Miyaji H, Izumi K, Sutton SJ, Miyamoto Y. J Phys Soc Jpn 1998;67:3338.
[5] Mareau VH, Prud'homme RE. Macromolecules 2005;38:398.
[6] Taguchi K, Miyaji H, Izumi K, Hoshino A, Miyamoto Y, Kokawa R. J Macromol Sci Phys 2002;B41:1033.

[7] Hall DB, Underhill P, Torkelson JM. Polym Eng Sci 1998;38:2039.
[8] Schubert DW, Dunkel T. Mater Res Innovations 2003;7:314.
[9] Barnes KA, Karim A, Douglas JF, Nakatani AI, Gruell H, Amis EJ. Macromolecules 2000;33:4177.
[10] Kressler J, Wang C, Kammer HW. Langmuir 1997;13:4407.
[11] Sehgal A, Ferreiro V, Douglas JF, Amis EJ, Karim A. Langmuir 2002; 18:7041.
[12] Stange TG, Evans DF. Langmuir 1997;13:4459.
[13] Lorenz-Haas C, Müller-Buschbaum P, Kraus J, Bucknall DG, Stamm M. Appl Phys 2002;A74:S383.
[14] Reiter G. Phys Rev Lett 2001;87:186101.
[15] Brochard-Wyart F, Daillant J. Can J Phys 1990;68:1084.
[16] Xie R, Karim A, Douglas JF, Han CC, Weiss RA. Phys Rev Lett 1998; 81:1251.
[17] Duvault Y, Gagnaire A, Gardies F, Jaffrezic-Renault N, Martelet C. Thin Solid Films 1990;185:169.
[18] Mareau VH, Prud'homme RE. Macromolecules 2003;36:675.
[19] Schönherr H, Bailey LE, Frank CW. Langmuir 2002;18:490.
[20] Kikkawa Y, Abe H, Iwata T, Inoue Y, Doi Y. Biomacromolecules 2001;2:940.
[21] Kikkawa Y, Abe H, Fujita M, Iwata T, Inoue Y, Doi Y. Macromol Chem Phys 2003;204:1822.
[22] Izumi K, Ping G, Hashimoto M, Toda A, Miyaji H, Miyamoto Y, et al. In: Nishinaga T, Nishioka K, Harada J, Sasaki A, Takei H, editors. Advances in the understanding of crystal growth mechanisms. Amsterdam: Elsevier Science B.V.; 1997. p. 337–48.
[23] Persenaire O, Alexandre M, Degée P, Dubois P. Biomacromolecules 2001;2:288.
[24] Massa MV, Carvalho JL, Dalnoki-Veress K. Eur Phys J 2003;12:111.
[25] Massa MV, Dalnoki-Veress K. Phys Rev Lett 2004;92:255509.
[26] Hoffman JD, Davis GT, Lauritzen Jr JI. In: Hannay NB, editor. Treatise in solid state chemistry, vol. 3. New York: Plenum; 1976. p. 497–614.
[27] Keith HD, Padden Jr FJ. J Appl Phys 1963;34:2409.
[28] Vancso GJ, Beekmans LGM, Pearce R, Trifonova D, Varga J. J Macromol Sci Phys 1999;B38:491.
[29] Kimura K, Kobayashi K, Yamada H, Horiuchi T, Ishida K, Matsushige K. Jpn J Appl Phys 2004;43:4575.
[30] Mareau VH, Prud'homme RE. Macromolecules 2002;35:5338.
[31] Keith HD, Padden Jr FJ, Lotz B, Wittmann J-C. Macromolecules 1989;22:2230.
[32] Keith HD, Padden Jr FJ. Polymer 1984;25:28.
[33] Lotz B, Cheng SZD. Polymer 2005;46:577.